# Neutrons from nuclear capture of negative pions

R. Madey, T. Vilaithong,* B. D. Anderson, J. N. Knudson,† T. R. Witten,‡ and A. R. Baldwin
*Department of Physics, Kent State University, Kent, Ohio 44242*

F. M. Waterman§
*Department of Radiology, University of Chicago, Chicago, Illinois 60637*
(Received 30 June 1981)

We measured the energy spectra and yields of neutrons above 1.2 MeV from nuclear capture of negative pions slowing down and stopping in C, N, O, Al, Cu, Ta, and Pb targets. Each neutron spectrum was decomposed into an evaporation portion and a direct portion. The number of direct neutrons per stopped pion is substantially constant for all the targets with a mean value of $1.74\pm0.28$, whereas the yield of evaporation neutrons increases by an order of magnitude from about 0.7 for carbon to about 7 for lead. The total kinetic energy carried away by the neutrons is substantially constant also for all the targets with a mean value of $76.7\pm2.0$ MeV. The kinetic energy carried away by evaporation neutrons increases with mass number with an associated decrease in the kinetic energy carried away by direct neutrons. We obtained the nuclear temperature (in MeV) of the first residual nucleus formed in the evaporation process for each target: Pb (1.4), Ta (1.4), Cu (1.9), Al (2.3), O (2.2), N (2.2), and C (2.1). The spectrum from a light target displays a shoulder in the region around 60 MeV which is consistent with a two-nucleon absorption mechanism. The direct neutron spectra are characterized by a rising yield as the neutron energy decreases in the region from 30 MeV down to about 10 MeV. The data are compared with previous measurements and with the predictions of intranuclear cascade and preequilibrium calculations.

[NUCLEAR REACTIONS C, N, O, Al, Cu, Ta, Pb $(\pi^-,xn)$, $E_{\pi^-}\approx0$ MeV. Measured differential energy spectra and yields. Deduced nuclear temperature. Compared results to intranuclear cascade and preequilibrium model calculations.]

## I. INTRODUCTION

Calculations[1–4] of the neutron energy spectrum emitted from an atomic nucleus that captures a slow negative pion do not agree either with experiment or with each other over the entire range of emitted neutron energies. Attempts to determine which calculations provide correct results in any part of the spectrum have been complicated by the fact that the available experimental measurements[5–8] of neutron energy spectra do not agree for those cases where the same targets were studied. The calculations typically follow the Monte Carlo method of the intranuclear cascade model for predicting the neutron yields in the high-energy portion of the spectrum and include an additional yield at lower energies from an evaporation model calculation. The basic assumption about the pion absorption process is that the pion capture occurs on a pair of nucleons in the nucleus.[9] In order to resolve the discrepancies between available experimental measurements and in order to provide accurate and reliable data for comparison with calculations, we measured neutron energy spectra from negative pions slowing down and stopping in several target materials. Measurements of the energy spectra and yields of neutrons from targets which comprise biological systems are important also for assessing the unwanted neutron dose delivered during pion radiotherapy.

Several authors reported measurements of neutron spectra from capture of negative pions in various targets. These targets include nuclear emulsion (Barkow *et al.*[10]); carbon, aluminum, cadium, lead,

 

and uranium (Anderson *et al.*[5]); copper, tin, and lead ( Venuti *et al.*[6]); lithium-6, lithium-7, carbon, nitrogen, copper, and lead (Hattersley *et al.*[7]); and carbon and holmium (Dey *et al.*[8]). Also Dey *et al.* measured but did not publish spectra from tantalum and gold, and Hattersley *et al.* measured but did not publish spectra from oxygen, magnesium, aluminum, and sulfur. Since the "meson factories" became operational, Hartmann *et al.*[11] reported measurements on the energy spectra of neutrons emitted from the capture of negative pions stopping in carbon, cobalt, and gold, and Klein *et al.*[12] reported measurements from carbon, nitrogen, and oxygen.

Anderson *et al.*, Venuti *et al.*, Hattersley *et al.*, and Dey *et al.*, used time-of-flight techniques; however, the energy resolution in the measurements of Anderson *et al.* were poor in comparison with the others. Anderson *et al.* measured the neutron spectra from about 2 to 100 MeV with a resolution varying from 32 percent at 10 MeV to 94 percent at 100 MeV. Venuti *et al.* measured neutron spectra from 1 to 50 MeV with an energy resolution varying from 3 to 10 percent. The energy resolution in the measurements of Hattersley *et al.* varied from 11 percent at 10 MeV to 36 percent at 100 MeV, whereas the energy resolution in the measurements of Dey *et al.* varied from 7 percent at 10 MeV to 16 percent at 100 MeV. Hartmann *et al.*[11] measured the neutron spectra from 1 to 150 MeV with an energy resolution varying from 5 to 16 percent, and Klein *et al.*[12] measured neutron energy spectra above about 2.5 MeV with an energy resolution varying from 10 percent at threshold to about 30 percent at 100 MeV.

The measurements performed before the meson factories became operational are generally in poor agreement whenever a common target was studied; for example, the neutron energy spectra of Hattersley *et al.*, Anderson *et al.*, and Dey *et al.* for a carbon target all have different shapes and disagree in magnitude by factors of 2 or more. Similar discrepancies are observed in the comparisons of the measurements of Anderson *et al.*, Venuti *et al.*, and Hattersley *et al.* for a lead target. The more recent measurements of Hartmann *et al.* and Klein *et al.* are in better agreement with each other for a carbon target than any pair of earlier measurements; however, discrepancies of up to 30% are still observed in parts of the neutron spectrum. These two more recent measurements do not agree well with any of the earlier results. Because both of the more recent results were obtained at the same laboratory, and because significant discrepancies still exist, the measurements reported here provide an important separate determination of these spectra.

## II. EXPERIMENTAL PROCEDURE

The experimental arrangement is shown in Fig. 1. A negative pion beam with a momentum of 125 MeV/$c$ from a low-momentum pion-muon channel of the Nevis Laboratories synchrocyclotron was incident on a counter telescope. Pions came to rest in the target. A stopped pion was identified by a count in (NE-102) plastic scintillation detectors $S1$, $S2$, and $S3$ upstream of the target, and the absence of a count in the (NE-102) scintillation detector $S4$ downstream of the target. A (Pilot 425) threshold Cerenkov counter $C$ vetoed electrons in the beam. Since the range of a muon is greater than that of a pion of the same momentum, muons in the beam did not stop in the target and were vetoed by counter $S4$. Scintillator $S3$ was only 0.8 mm thick in order to minimize the number of pions stopped in it. The physical dimensions (in cm) of each counter were: $S1$ ($10.2\times10.2\times0.6$), $S2$ ($7.6\times7.6\times0.3$), $S3$ ($7.6\times7.6\times0.08$), $S4$ ($20.3\times20.3\times0.6$), and $C$ ($8.9\times8.9\times8.9$). Scintillators $S1$, $S2$, and $S3$ were viewed by 5.1 cm diam (RCA 8575) photomultiplier tubes (PMT) through tapered Lucite light pipes. Scintillator $S4$ was coupled to a 5.1 cm diam (Amperex 56 DVP) PMT by means of an adiabatic Lucite light pipe. The (Pilot 425) material of the Cerenkov counter was tapered at the base and was coupled directly to an RCA 8575 PMT.

The target was positioned at 45° relative to the incident pion beam. Targets of C, $N_2H_4$ (hydrazine), $H_2O$, Al, Cu, Ta, and Pb were 1.39, 1.28, 1.27, 1.72,

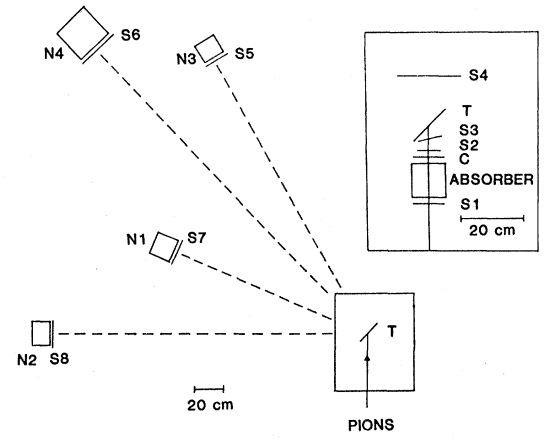


FIG. 1. Experimental arrangement.

2.83, 2.64, and 3.60 g/cm$^2$ thick, respectively. The areal dimensions of each target were 14.0 by 10.2 cm. Water was enclosed in a Lucite frame with 0.076 mm thick Mylar windows, and the hydrazine cell was an aluminum frame with 0.051 mm thick aluminum windows.

Neutrons were detected in NE-102 plastic scintillation detectors $N2$, $N3$, $N4$, and NE-213 liquid scintillator $N1$. Detectors $N2$ and $N3$ were 12.7 cm diam by 10.2 cm thick cylinders directly coupled to Amperex-type 58 DVP 12.7 cm photomultiplier tubes. Detector $N4$ was a 22.9 cm diam by 20.3 cm thick plastic cylinder viewed through a tapered Lucite light pipe by an Amperex 58 DVP photomultipler tube; an aluminum housing combined the photomultipler base, the photomultiplier tube, the magnetic shield, the light pipe, and the scintillator into a single unit as described by Madey and Waterman.[13] Detector $N1$ was a 12.7 cm diam by 12.7 cm thick NE-213 liquid cylinder and was directly coupled to an Amperex 58 DVP photomultiplier tube. The flight paths from the target were 1.35 m for $N1$, 2.0 m for $N2$ and $N3$, and 2.52 m for $N4$. The angles of these counters with respect to the direction of the incident pion beam were 65°, 85°, 25°, and 45° for $N1$, $N2$, $N3$, and $N4$, respectively. The energy of a neutron was determined from the measured time difference between the passage of the pion through counter $S3$ and the detection of the neutron in one of the four neutron counters. Anticoincidence detectors $S5$, $S6$, $S7$, and $S8$ were (0.6 cm thick NE-102) plastic scintillation counters which vetoed charged particles from the target. We did not use any local shielding near the neutron counters since in a preliminary run we detected low-energy neutrons scattered from local shielding material into the neutron counters.

Photomultiplier tube bases with a wide dynamic range[14] were used on counters $N2$, $N3$, and $N4$. A commercial (Ortec 270) photomultiplier base was used on the NE-213 counter $N1$ to produce direct anode and preamplified dynode signals for time-of-flight (TOF) and pulse-shape discrimination (PSD) purposes, respectively. Since this counter $N1$ was used to measure neutrons in the 1 to 40 MeV energy region, we incorporated a commerical pulse-shape-discrimination system, which is based on a zero-crossover method,[15,16] into the main electronics system to reduce the $\gamma$-ray background. Constant-fraction-timing discriminators were used on each neutron counter and on the timing counter $S3$.

We used an electronic scheme for multiparameter data acquisition analogous to the two-parameter system that has been described previously[14]; however, for our present measurements we recorded an additional parameter, namely, the PSD datum for counter $N1$. For each event, the following data were recorded on magnetic tape: (1) the pulse-height from each neutron counter, (2) the time interval between the passage of a particle through counter $S3$ and the detection of a particle in one of the neutron counters, (3) the PSD datum for counter $N1$, and (4) a tag word identifying a particular neutron counter. The data-acquisition system consisted of a Digital Equipment Corporation (DEC) PDP-11/15 computer with 28 K 16-bit words of core memory for programming and 32 K 24-bit words of core memory for data storage. The data-acquisition system enabled time-of-flight, pulse-height, and neutron-gamma pulse-shape histograms to be accumulated for on-line inspection and analysis.

The pulse height from each neutron counter was calibrated in about 12-h intervals with a series of radioactive gamma sources, namely $^{137}$Cs, $^{22}$Na, and $^{228}$Th. The Compton peak in the gamma-ray spectrum was used as a calibration point. We associated the peak channel with an electron energy equal to 0.95 that of the maximum Compton energy.[17] The pulse-height threshold of counter $N1$ was set at 105 keV equivalent-electron ($\simeq$720 keV proton) energy. The discriminator thresholds for the other three counters were set at 1 MeV equivalent-electron ($\simeq$3 MeV proton) energy.

The time-to-amplitude converter (TAC) for the time-of-flight spectrum was calibrated with a (Tennelec TC 850) precision time calibrator. The time calibration was 182 psec per channel over 2048 channels.

Prior to the TOF measurements, a differential range curve was taken to determine the beam momentum resolution and the absorber thickness to be used. The momentum resolution of the pion beam was found to be $\pm$4% and a Lucite absorber of thickness 3.8 cm (= 4.5 g/cm$^2$) cleanly separated the stopped pions and muons.

## III. TIME-OF-FLIGHT MEASUREMENTS

Time-of-flight (TOF) spectra were recorded simultaneously for the four neutron counters. A typical TOF spectrum from an aluminum target is shown in Fig. 2 for counter $N4$. This spectrum was constructed with a pulse-height threshold of 2.5 MeV equivalent-electron energy. In Fig. 2 the

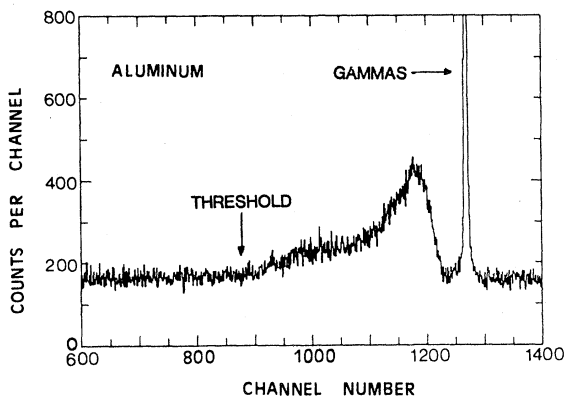


FIG. 2. Typical time-of-flight spectrum.

broad bump is the neutron time-of-flight spectrum; the narrow peak to the right of the broad bump is generated by prompt $\gamma$ rays. The TOF spectra for all counters display time-independent (flat) backgrounds before and after the spectral region of interest. The level of the background in the region below the discrimination threshold on the slow side of the neutron time-of-flight spectrum is typically 7 percent higher than that on the fast side of the spectrum earlier than the gamma peak. We attributed the excess events on the slow side of the spectrum to target-induced background from neutrons scattered in the surrounding materials (e.g., the floor and the accelerator shielding blocks) into the neutron counter. Each counter was mounted on a steel frame stand at a height of 1.8 m above the floor. Kinematically, if a neutron from the target is scattered from the floor into the NE-102 counters, it would be recorded in the TOF spectrum in the region below 28 MeV for $N2$ and $N3$ and below 37 MeV for $N4$. Neutrons scattered from the floor into the NE-213 counter $N1$ would contaminate the TOF spectrum in the region only below 8 MeV. For the NE-102 counters, we determined the level of the background by extrapolating the flat region on the slow side of the region of interest to 40 MeV (where floor scattering could first appear); then we extrapolated the flat region on the fast side of the spectrum to the center of the prompt gamma-ray peak, and we connected these two regions by extrapolating linearly from the height of the flat region at 40 MeV to the center of the prompt gamma-ray peak. A similar procedure was applied to the near (NE-213) counter $N1$ with the flat region on the slow side of the spectrum being extrapolated up to 8 MeV. The assumed shape of the background underneath a neutron spectrum is consistent with the shape observed for room-scattered neutron backgrounds measured with shadow shields to attenuate the direct neutron flux for similar measurements of neutron spectra.[18,19] It is important to note, since the background levels are only slightly ($\leq 7\%$) different on the fast and slow sides of the TOF spectra, the difference between the assumed shape for the background subtraction and a single linear subtraction is a second-order correction.

When the PSD system was not enabled, the background from the near counter $N1$ did exhibit some structure which appeared in the neutron energy region above 10 MeV. Recall that the hardware threshold of this counter was set at only about 105 keV electron-equivalent energy in order to detect neutrons in the energy region from about 1 to 40 MeV. With the window in the $n$-$\gamma$ PSD system set to accept only gamma rays, the TOF spectrum from $N1$ revealed that his background was mostly low-energy gamma rays. The PSD system rejected these background gamma rays.

When we increased the absorber thickness to allow muons to stop in the lead target, we observed no structure in the TOF spectrum except for a prompt x-ray peak; this test indicated that the observed neutrons originated from negative pions stopping in the target. Also we made measurements with the target mounting stand only and with blank target cells. In these tests with the main target removed, we obtained a measure of the number of pions that stop in counter $S3$ and in the mounting hardware. While these neutron spectra (taken without the main target) resembled the carbon spectrum, the contribution of $S3$ and the mounting hardware was less than five percent of that with a carbon target in place. The neutron spectrum from each target was corrected by subtracting a carbon-type spectrum contributed by $S3$ and the mounting hardware. Note that the contribution of $S3$ and the mounting hardware decreases to a fraction of a percent of the low-energy yield from a heavy target.

Several runs were made with a total of at least $10^3$ pions stopped in each target. The method of data reduction is described in the next section.

## IV. DATA REDUCTION

The differential neutron spectrum $N(T)$ in units of neutrons per stopped pion per MeV for each energy interval $\Delta T$ of the spectrum is given by the expression:

$$N(T)=\frac{4\pi R(T)}{\Delta\Omega N_{\pi}\epsilon(T)\Delta T}\,, \tag{1}$$

where $R(T)$ is the number of real neutron counts within an energy interval of width $\Delta T$, $\Delta\Omega$ is the solid angle subtended by a neutron detector, $N_\pi$ is the number of stopped pions, and $\epsilon(T)$ is the detection efficiency of the counter for a neutron with a mean kinetic energy $T$. The width $\Delta T$ of the energy interval was taken to be equal to the system energy resolution (FWHM) calculated for the mean energy of the interval. The energy resolution $(\Delta T/T)$ of the system is calculated from the expression:

$$\frac{\Delta T}{T}=\gamma(\gamma+1)\left[\left[\frac{\Delta x(1-\beta n)}{x}\right]^2+\left[\frac{\Delta t}{t}\right]^2\right]^{1/2}, \tag{2}$$

where $\Delta x$ is the uncertainty in the neutron flight path, $\beta$ is the neutron speed in units of the speed of light, $n$ is the refractive index of the scintillator, and $\Delta t$ is the intrinsic time dispersion of the system. The factor $\beta n$ is included to account for the finite speed of light in the scintillator. The time resolution of the system was taken to be equal to the observed width (FWHM) of the prompt gamma-ray peak from the lead target. The time resolution was 1.5 nsec (FWHM) for counter $N4$ and 1.1 nsec for the other three counters. The energy resolution varied from 13 percent at 10 MeV to 18 percent at 100 MeV for counter $N4$ and 9 percent at 10 MeV to 17 percent at 100 MeV for counters $N2$ and $N3$.

The solid angle $\Delta\Omega$ was determined from the calculated mean neutron flight path. The average position of interaction in the neutron counter is energy dependent because it depends on the neutron mean free path. This average position was calculated for each energy bin using the probability distribution of neutron path lengths within the detector. The mean neutron flight path was thus equal to the distance from the target to the front face of the detector plus the mean interaction length within the detector.

The neutron detection efficiency $\epsilon(T)$ was calculated with the Monte Carlo computer program of Cecil *et al.*[20] which is an improved version of the program written by Stanton.[21] The improvements include new cross section determinations for the inelastic reactions on carbon, a proper determination of the energy deposited by escaping charged particles, the adoption of new light-response functions, and the use of relativistic kinematics. These improvements are especially important for neutron energies above about 30 MeV. These calculations were improved further for low threshold settings by adding an explicit evaporation peak for the $^{12}C(n,np)$ reaction channel which dominates the detection process for incident neutron energies above about 40 MeV. The evaporation contribution was assumed to be uniform in emitted proton energy from 0 to 10 MeV. The strength was taken to be consistent with the recent $^{12}C(n,xp)$ measurements of Brady *et al.*[22] at 27.4, 39.7, and 60.7 MeV and the earlier measurements of Kellogg[23] at 90 MeV. The light output function for the NE-213 scintillator was a semiempirical fit to the data of Verbinski *et al.*[24] and Czirr *et al.*[25]; that for NE-102, a semiempirical fit to the data of Madey *et al.*[26] The contribution to the counter efficiency from the inelastic $(n,n'\gamma)$ channel resulting from the interaction of $\gamma$ rays was not included in the calculations for the liquid NE-213 detector since the $\gamma$ rays were rejected by the PSD system. These efficiency calculations[20] provide good agreement with many experimental measurements of neutron detector efficiencies for neutron energies from about 1 to 300 MeV and for detector thresholds from about 0.1 MeV to about 22 MeV equivalent-electron energy. The uncertainty in the Monte Carlo calculation of the efficiencies is estimated to be about 4 percent for a well-known threshold. An uncertainty estimated to be about 3 percent in the pulse-height threshold results in an additional uncertainty in the efficiencies of about 3 percent. A net uncertainty of 5 percent in the efficiency results from the quadrature sum of these two quantities. Efficiencies are listed in Table I for the NE-213 neutron counter and in Table II for the NE-102 neutron counters.

The neutron spectrum was determined from the measured TOF spectra in two separate energy regions. The low-energy portion from 1 to 40 MeV was determined from the data from the liquid scintillator $N1$, while the spectrum above 30 MeV was determined from the data from the other three counters. The two spectra joined smoothly in the overlap region. Data from the NE-213 scintillation detector above 1.8 MeV were analyzed for a pulse-height threshold of 200 keV equivalent-electron energy. Data from the NE-213 counter from 1.0 to 3.0 MeV were analyzed at the hardware threshold of 105 keV equivalent-electron energy and agreed with the higher threshold results in the overlap region above 1.8 MeV. In the 1 to 40 MeV neutron-energy region, we used pulse-shape discrimination to reject $\gamma$ rays. The $\gamma$ rejection was performed separately for each of twelve different pulse-height regions because the $\gamma$-rejection technique was pulse-height dependent. Since the neutron and gamma events began to overlap in the pulse-shape spectrum below 2 MeV, the PSD system could not

reject all gamma rays in that region; however, this fact does not alter the final result because we subtracted the time-independent gamma-ray background from the TOF spectrum. TOF analysis with and without PSD in this region gave the same result. The only effect of including gamma rays was to decrease the statistical accuracy. While the neutron and gamma-ray peaks in the PSD spectrum were better separated above 2 MeV, the separation was never quite complete and some neutrons were lost. The correction for this loss was never greater than 3 percent. In the 30 to 140 MeV region, the pulse-height threshold used for analysis was 2.5 MeV equivalent-electron energy for each NE-102 counter. The bin width was taken to be equal to the energy resolution (FWHM) of the 22.9 cm diam by 20.3 cm high counter. Data from counters $N2$ and $N3$ were summed and the resulting energy spectrum was combined with that obtained from counter $N4$.

Several corrections were made to the number of stopped pions and to the number of detected neutrons. In order to obtain the true pion stopping rate, the observed number of stopped pions was corrected for (1) the dead-time loss in the data-acquisition system, (2) the number of muons stopping in the target, (3) pion multiple scattering by the counter telescope, (4) pion decay in flight, and (5) pion capture by hydrogen nuclei in the water and hydrazine targets. The magnitudes of these corrections are listed in Table III. A correction for absorption of pions in flight when the pions traverse counter $S3$ was estimated to be less than 0.1 percent; therefore, this correction was neglected. The contribution from the charge-exchange reaction

$$^{A}Z(\pi^-,\pi^0 n)^{(A-1)}(Z-1)$$

is much smaller than 0.1 percent; hence, this correction was neglected also.

The measured neutron spectrum was corrected also for (6) neutron interactions in the target, (7) neutron interaction in the anticoincidence counter ahead of each counter, (8) neutrons emitted from pions captured by carbon nuclei in the thin scintillator $S3$ just ahead of the target, (9) neutron losses from the pulse-shape-discrimination requirement in counter $N1$, and (10) neutron interactions in the

TABLE I. Neutron detection efficiencies for a 12.7 cm diam by 12.7 cm thick NE-213 scintillator with discrimination thresholds of 105 and 200 keV equivalent-electron energy.

| Neutron kinetic energy (MeV) | Percent efficiency[a] 105 keV | 200 keV |
|---|---|---|
| 1.31 | 59.7 | |
| 1.56 | 63.1 | |
| 1.85 | 64.8 | 51.4 |
| 2.20 | 64.4 | 55.3 |
| 2.61 | 63.3 | 56.7 |
| 3.10 | (60.8) | 56.7 |
| 3.68 | (58.2) | 55.9 |
| 4.35 | (57.0) | 54.4 |
| 5.15 | (55.1) | 47.6 |
| 6.08 | (51.6) | 48.4 |
| 7.19 | (48.5) | 46.1 |
| 8.35 | (45.2) | 42.2 |
| 9.58 | (42.8) | 40.5 |
| 11.0 | (41.3) | 39.1 |
| 12.6 | (40.3) | 38.0 |
| 14.4 | (41.0) | 38.7 |
| 16.5 | (40.3) | 38.8 |
| 18.8 | (38.3) | 37.2 |
| 21.6 | (36.0) | 34.7 |
| 24.7 | (33.6) | 32.4 |
| 28.3 | (31.0) | 30.2 |
| 32.4 | (28.2) | 27.4 |
| 37.3 | (25.3) | 24.9 |

[a]The values in parentheses were not used in this work.

TABLE II. Neutron detection efficiencies for cylindrical NE-102 scintillators at a threshold of 2.5 MeV equivalent-electron energy.

| Neutron kinetic energy (MeV) | Percent efficiency 12.7 cm diam ×10.2 cm | 22.9 cm diam ×20.3 cm |
|---|---|---|
| 11.0 | 18.8 | 32.6 |
| 12.6 | 19.1 | 32.5 |
| 14.4 | 18.4 | 31.4 |
| 16.5 | 17.1 | 29.1 |
| 18.8 | 16.4 | 27.8 |
| 21.6 | 15.2 | 26.5 |
| 24.7 | 16.6 | 29.1 |
| 28.3 | 18.1 | 32.6 |
| 32.4 | 18.2 | 33.1 |
| 37.3 | 18.2 | 33.8 |
| 42.9 | 18.0 | 32.7 |
| 49.6 | 17.2 | 31.3 |
| 57.7 | 16.1 | 29.2 |
| 67.4 | 14.4 | 27.2 |
| 79.3 | 13.4 | 24.8 |
| 94.4 | 12.5 | 23.4 |
| 114 | 11.5 | 22.0 |
| 140 | 11.2 | 21.1 |

TABLE III. Corrections to the measured number of stopped pions and number of detected neutrons.

| | Correction | Magnitude (%) |
|---|---|---|
| (1) | Dead-time loss in the data-acquisition system | 9.1—19.0 |
| (2) | Muons that stop in the target | 1.6—2.5 |
| (3) | Pion multiple scattering by the counter telescope | 1.2 |
| (4) | Pion decay in flight between counter $S3$ and the target | 1.0 |
| (5) | Charge-exchange and radiative pion capture by hydrogen nuclei (Ref. 21) in | |
| | (a) the water target | 0.35 |
| | (b) the hydrazine target | 0.59 |
| (6) | Neutron interactions in | |
| | (a) nonhydrogenous targets | $<3$ |
| | (b) hydrogenous targets | 0.5—12 |
| (7) | Neutron interactions in the anticoincidence counter | |
| | (a) ahead of NE-213 detector $N1$ | 2—12 |
| | (b) ahead of NE-102 detectors $N2$, $N3$, and $N4$ | 1—5 |
| (8) | Pions that stop in counter $S3$ ahead of the target | 4.5 |
| (9) | Neutron loss in the PSD system ($N1$) | 0.6—2.8 |
| (10) | Neutron interactions in the aluminum casing of counter $N4$ | 0.5—1.3 |

aluminum casing of counter $N4$. The magnitudes of these corrections are listed also in Table III.

The overall systematic error for the absolute value of the neutron yield is estimated to be $\pm 6.3$ percent. This number was obtained from the following estimated uncertainties summed in quadrature: (1) $\pm 5$ percent for the neutron detection efficiency; (2) $\pm 2.5$ percent for neutron interactions in the target; (3) $\pm 2.6$ percent for neutron interactions in the anticoincidence counter; (4) $\pm 0.3$ percent for neutron interactions in the neutron counter aluminum casing; (5) $\pm 1.1$ percent for muons stopping in the target; (6) $\pm 0.3$ percent for pion multiple scattering; (7) $\pm 0.7$ percent for neutron losses in the PSD system; and (8) $\pm 0.3$ percent for pions stopping in counter $S3$.

## V. EXPERIMENTAL RESULTS

The neutron energy spectra obtained from our measurements are tabulated in Table IV. In Fig. 3, we compare our spectra from carbon, copper, and lead. The spectra above 10 MeV are substantially the same for copper and lead, but the carbon target reveals more neutrons in the region from about 40 to 80 MeV. The spectra differ below 10 MeV with more neutrons coming from the heavier target. In Fig. 4, we present a similar comparison of our spectra from nitrogen, aluminum, and tantalum. The nitrogen target reveals more neutrons than the tantalum target in the higher-energy portion of the spectrum above about 50 MeV. The increased number of neutrons in this energy region for light targets is consistent with a two-nucleon absorption process. Neutron emission at about 60 MeV results when two neutrons share an energy equal approxi-

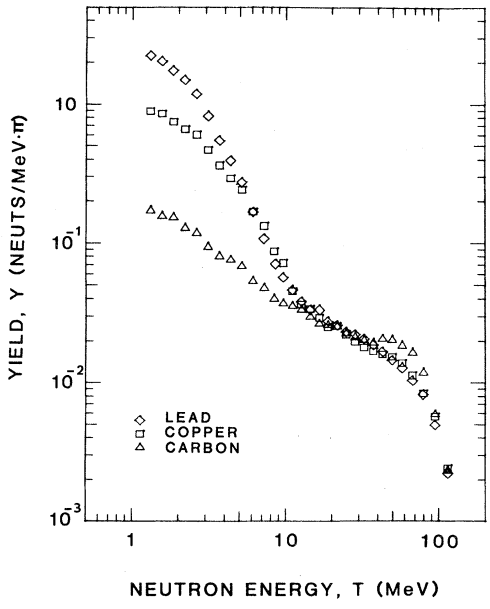


FIG. 3. Neutron spectra from negative pions stopped in carbon, copper, and lead.

TABLE IV. Neutron energy spectra resulting from negative pion capture in various targets.

| | Neutrons per MeV per 100 pions stopped in the target.[a] | | | | | | |
|---|---|---|---|---|---|---|---|
| $T$ (MeV) | C | N | O | Al | Cu | Ta | Pb |
| 1.31 | 17.10(1.40) | 24.50(1.40) | 21.40(1.10) | 32.70(1.40) | 89.00(2.20) | 199.00(2.00) | 223.00(3.00) |
| 1.56 | 15.60(1.10) | 19.50(1.10) | 17.80(0.90) | 35.70(1.10) | 85.60(1.80) | 172.00(2.00) | 205.00(2.00) |
| 1.85 | 15.30(0.90) | 18.20(0.80) | 18.20(0.70) | 32.30(0.90) | 74.50(1.40) | 147.00(2.00) | 174.00(2.00) |
| 2.20 | 12.80(0.60) | 16.30(0.60) | 16.40(0.50) | 31.00(0.70) | 65.90(1.20) | 125.00(1.00) | 150.00(2.00) |
| 2.61 | 11.80(0.50) | 14.90(0.50) | 15.40(0.40) | 26.70(0.50) | 60.10(0.90) | 99.80(1.00) | 118.00(1.00) |
| 3.10 | 9.35(0.37) | 12.00(0.40) | 12.40(0.30) | 21.30(0.50) | 46.80(0.70) | 73.20(0.40) | 82.10(1.00) |
| 3.68 | 7.99(0.31) | 10.50(0.30) | 9.95(0.26) | 18.90(0.40) | 36.10(0.60) | 51.70(0.60) | 54.40(0.80) |
| 4.35 | 7.55(0.26) | 8.69(0.25) | 8.60(0.22) | 15.30(0.30) | 29.10(0.50) | 37.40(0.50) | 38.90(0.60) |
| 5.15 | 6.82(0.25) | 8.31(0.24) | 8.24(0.21) | 13.60(0.30) | 24.30(0.40) | 29.40(0.40) | 27.30(0.50) |
| 6.08 | 5.34(0.20) | 6.71(0.19) | 6.63(0.17) | 10.20(0.20) | 16.80(0.30) | 18.50(0.30) | 16.60(0.40) |
| 7.19 | 4.76(0.18) | 5.80(0.17) | 5.39(0.14) | 8.05(0.19) | 13.30(0.30) | 12.30(0.30) | 10.70(0.30) |
| 8.55 | 3.99(0.18) | 4.87(0.17) | 4.63(0.14) | 6.34(0.18) | 8.73(0.25) | 8.10(0.22) | 7.05(0.27) |
| 9.58 | 3.69(0.16) | 4.47(0.15) | 4.50(0.12) | 5.62(0.17) | 7.20(0.22) | 6.63(0.19) | 5.70(0.24) |
| 11.00 | 3.54(0.14) | 3.95(0.13) | 4.08(0.11) | 4.60(0.14) | 4.53(0.18) | 4.52(0.13) | 4.61(0.20) |
| 12.60 | 3.35(0.13) | 3.69(0.11) | 3.68(0.10) | 4.06(0.13) | 3.65(0.15) | 3.96(0.14) | 3.79(0.18) |
| 14.40 | 2.96(0.11) | 3.30(0.10) | 3.11(0.08) | 3.59(0.11) | 3.38(0.13) | 3.49(0.12) | 3.32(0.15) |
| 16.50 | 2.64(0.10) | 2.79(0.08) | 2.92(0.07) | 3.35(0.10) | 2.92(0.11) | 3.15(0.10) | 3.33(0.14) |
| 18.80 | 2.59(0.09) | 2.60(0.08) | 2.71(0.07) | 2.72(0.08) | 2.51(0.10) | 2.65(0.08) | 2.75(0.12) |
| 21.60 | 2.53(0.08) | 2.57(0.07) | 2.56(0.06) | 2.43(0.08) | 2.56(0.09) | 2.66(0.08) | 2.58(0.11) |
| 24.70 | 2.24(0.07) | 2.32(0.06) | 2.26(0.06) | 2.17(0.07) | 2.22(0.08) | 2.12(0.07) | 2.31(0.10) |
| 28.30 | 2.11(0.07) | 2.19(0.06) | 2.17(0.05) | 2.07(0.06) | 1.97(0.08) | 2.04(0.07) | 2.20(0.09) |
| 32.40 | 2.02(0.07) | 2.07(0.05) | 2.11(0.05) | 1.96(0.06) | 1.79(0.07) | 1.89(0.06) | 2.06(0.06) |
| 37.30 | 1.93(0.06) | 1.95(0.04) | 2.00(0.04) | 1.81(0.05) | 1.69(0.06) | 1.75(0.06) | 1.87(0.05) |
| 42.90 | 2.06(0.05) | 1.89(0.04) | 1.94(0.03) | 1.69(0.04) | 1.59(0.05) | 1.73(0.05) | 1.67(0.04) |
| 49.60 | 2.02(0.04) | 1.79(0.03) | 1.87(0.03) | 1.67(0.04) | 1.54(0.04) | 1.50(0.04) | 1.44(0.04) |
| 57.70 | 1.85(0.04) | 1.69(0.03) | 1.78(0.03) | 1.52(0.03) | 1.38(0.04) | 1.38(0.03) | 1.28(0.03) |
| 67.40 | 1.64(0.03) | 1.46(0.03) | 1.58(0.03) | 1.24(0.03) | 1.13(0.03) | 1.13(0.03) | 1.03(0.03) |
| 79.30 | 1.18(0.03) | 1.08(0.02) | 1.13(0.02) | 0.95(0.02) | 0.84(0.03) | 0.83(0.03) | 0.82(0.02) |
| 94.40 | 0.59(0.02) | 0.62(0.02) | 0.62(0.02) | 0.58(0.02) | 0.57(0.02) | 0.49(0.02) | 0.50(0.02) |
| 114.00 | 0.23(0.01) | 0.24(0.01) | 0.25(0.01) | 0.23(0.01) | 0.24(0.01) | 0.22(0.01) | 0.22(0.01) |
| 140.00 | 0.00(0.00) | 0.00(0.00) | 0.00(0.00) | 0.00(0.00) | 0.02(0.01) | 0.02(0.01) | 0.01(0.01) |

[a]Uncertainties shown are statistical only. The overall systematic uncertainty is ±6.3 percent, as discussed in the text.

mately to the pion rest energy minus the neutron separation energy. The decrease in the neutron yield in this energy region for heavier targets (e.g., copper, tantalum, and lead) arises partly because as the nucleon number increases, it is less likely that neutrons emitted in the capture on a two-nucleon pair will escape the nucleus without undergoing a secondary interaction. Our spectra from oxygen (not plotted) and nitrogen are identical to each other within experimental errors. The carbon spectrum above 10 MeV is identical also to that from either oxygen or nitrogen except that the shoulder in the region around 60 MeV is more evident in the carbon spectrum. Also the yield of neutrons below 10 MeV from carbon is slightly lower than that from either oxygen or nitrogen.

In Fig. 5, we compare our measurements from carbon with those of Hartmann *et al.*[11] and Klein *et al.*[12] The three different sets of measurements generally agree to within 20 to 30%. In the pre-"meson-factory" experiments, much larger discrepancies were observed. The measurements of Hartmann *et al.* generally agree with our results at low energies (below about 8 MeV) and at high energies (above about 60 MeV). In the intermediate region, the results of Hartmann *et al.* are lower by 20 to 30%. In contrast, the results of Klein *et al.* are generally lower at high energies, but agree with our measurements from about 20 to 40 MeV.

We attribute part of the discrepancies to different

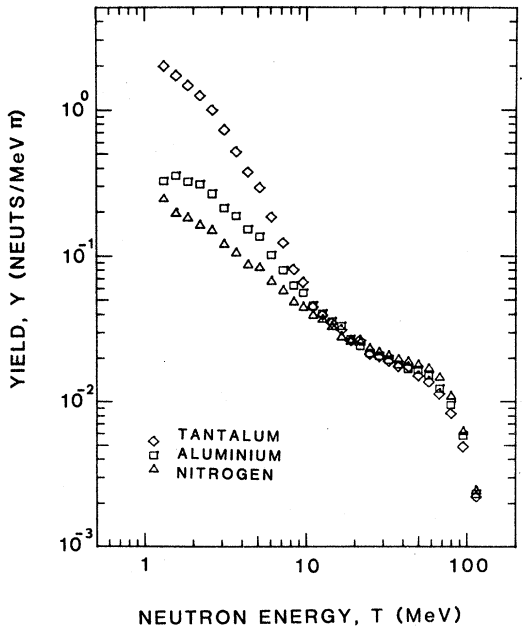


FIG. 4. Neutron spectra from negative pions stopped in nitrogen, aluminum, and tantalum.

determinations of the neutron detector efficiencies. Hartmann *et al.* calculated the neutron detection efficiency from 1 to 50 MeV with the Monte Carlo computer code 05-S (from the Oak Ridge National Laboratory). This code does not properly account for escaping recoil particles and uses an earlier data base for the various neutron-induced cross sections. The efficiencies calculated from this code are likely unreliable above about 30 MeV where the inelastic reactions on carbon begin to dominate and also

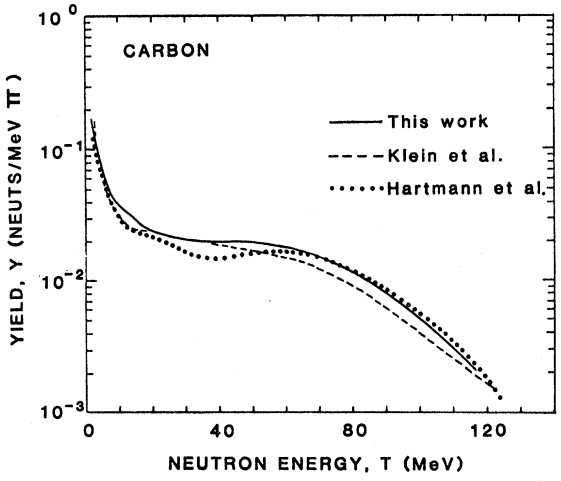


FIG. 5. Neutron spectrum from negative pion capture in carbon. The data of Hartmann *et al.* (Ref. 11) and Klein *et al.* (Ref. 12) are shown for comparison.

where escaping charged-particles are significant. At energies above 50 MeV, Hartmann *et al.* extrapolated the efficiency from a measured value at 70 MeV according to an inverse power law in the neutron kinetic energy. This extrapolation is an oversimplification of the high-energy behavior. Klein *et al.* calculated the neutron detection efficiency with the Monte Carlo computer code of Stanton.[21] The code of Cecil *et al.*[20] is a substantially improved version of the original Stanton code which also suffers from the same two basic problems as the 05-S computer code. The Stanton code calculations are also less reliable above about 30 MeV.

We used the improved code of Cecil *et al.* to calculate the efficiencies for the neutron detectors of Hartmann *et al.* and also for those of Klein *et al.* In Fig. 6 we show the comparison of our calculated efficiencies with their published calculations. Note that 20 to 30% differences are observed in some regions. In Fig. 7 we compare our measurements with those of Hartmann *et al.* and Klein *et al.* after the latter were adjusted to incorporate our calculated efficiencies for their detectors. The general agreement between the three different sets of mea-

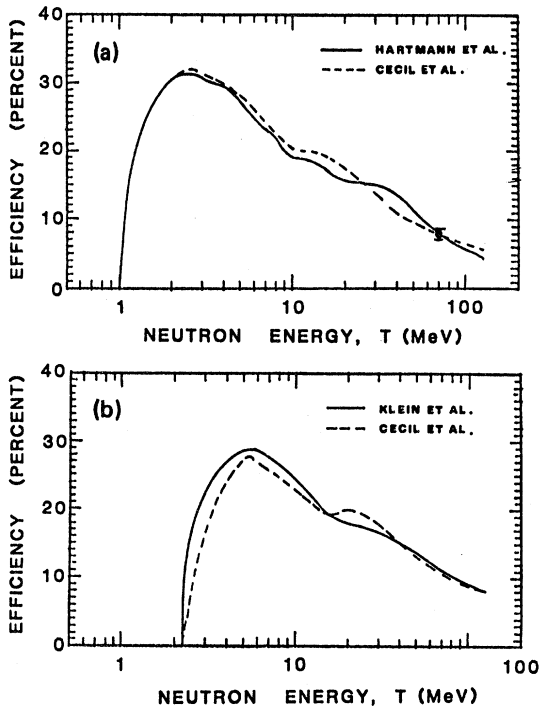


FIG. 6. Calculated neutron detection efficiencies as originally reported and as calculated with the modified code of Cecil *et al.* (Ref. 20) for (a) the 11.7 cm diam by 4.6 cm high NE-213 counter of Hartmann *et al.* (Ref. 11) and (b) the 7.5 cm diam by 7.5 cm thick NE-123 counter of Klein *et al.*[12]

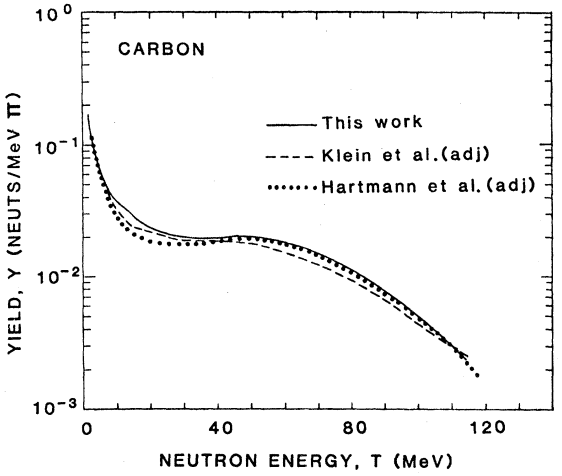


FIG. 7. Neutron spectrum from negative pion capture in carbon. The spectra of Hartmann *et al.* (Ref. 11) and Klein *et al.* (Ref. 12) "adjusted" to use efficiencies calculated with the modified code of Cecil *et al.* (Ref. 20) are shown for comparison (see text).

surements is improved by common efficiency calculations. The general agreement below 8 MeV is maintained (and perhaps improved slightly). The good agreement of the results of Hartmann *et al.* with our measurements above about 60 MeV is also maintained, although the Hartmann *et al.* results are now slightly lower (rather than slightly higher) than our results. The adjusted measurements of Klein *et al.* are still somewhat lower than our measurements in the high-energy region, but are now less so. The agreement of the three different sets of measurements is improved also in the intermediate energy region from 10 to 60 MeV. The adjusted results of Hartmann *et al.* are still significantly lower than than our results in this region with a maximum difference of about 15% near 20 MeV. The adjusted measurements of Klein *et al.* appear to approximately split the difference between the other two sets of measurements in this intermediate energy region.

It is important to realize that these three sets of measurements (even without the use of a common efficiency calculation) agree much better than any *two* of the earlier sets of measurements. We attribute the discrepancies to the use of different efficiency calculations and to differences in background subtractions. Figure 7 shows the overall good agreement obtained using the same efficiency calculations. The largest remaining discrepancies, which are in the intermediate energy region from 10 to 40 MeV, probably result from differences in the backgrounds subtracted; for example, Hartmann *et al.* reported that the target-correlated backgrounds represented more than 50 percent of the total background in the region between 10 and 15 MeV. They made measurements with shadow bars to subtract this background. We did not observe such large target-correlated backgrounds and do not expect room-scattered neutrons to contribute significantly in our measurements above 8 MeV. As discussed earlier in Sec. III, the reason is that neutrons scattered from the floor represent the dominant contribution to room-scattered backgrounds, and the highest-energy neutrons produced in the target and scattered by the floor would appear below 8 MeV in the NE-213 counter spectrum. The NE-213 counter was used to measure the spectrum up to 30 MeV. The NE-102 counters, used to measure the spectrum above 30 MeV, would see floor-scattered neutrons only *below* 30 MeV.

## VI. NUCLEAR TEMPERATURE

If we assume that the measured neutron spectra consist of *direct* neutrons and *evaporation* neutrons, we can fit the evaporation portion of the spectrum with the expression of Le Couteur[27]:

$$N(T) \propto T^{5/11} \exp\left[-\frac{12}{11}\frac{T}{\tau}\right] . \tag{3}$$

Here $N(T)$ is the number of neutrons per stopped pion per MeV, $T$ is the neutron kinetic energy, and $\tau$ is the temperature of the first residual nucleus formed in the evaporation.

In Fig. 8, we present a semilogarithmic plot of the differential neutron yield in the evaporation region divided by $T^{5/11}$ for lead, copper, aluminum, and carbon targets. The fact that the data fall on straight lines confirms the exponential nature of the fit in the region from about 1.2 to 4.0 MeV. From the slope of these curves, we deduced the following values for the nuclear temperature (in MeV): Pb (1.4), Ta (1.4), Cu (1.9), Al (2.3), O (2.2), N (2.2), and C (2.1). Figure 9 is a plot of the nuclear temperature versus the mass number of the target nucleus. The fitting procedure yielded statistical uncertainties of less than $\pm 0.2$ MeV for C, N, O, and Al, and less than $\pm 0.1$ MeV for Cu, Ta, and Pb. In addition to the uncertainty from the fitting procedure, there exist additional uncertainties for possible background contributions and relative errors in the efficiency calculations which could change the slope of the data at low energies. From these con-

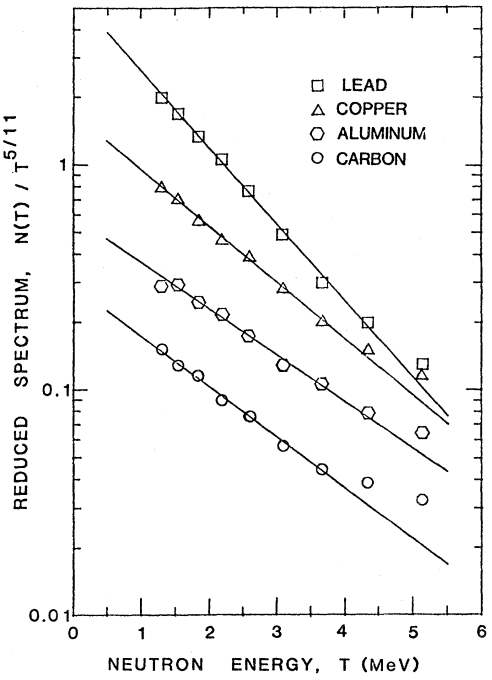


FIG. 8. Reduced neutron spectra for lead, copper, aluminum, and carbon versus the neutron kinetic energy in the region from 1 to 6 MeV.

siderations we estimate the overall uncertainties in the nuclear temperatures to be $\pm 0.2$ MeV.

We note that the nuclear temperatures reported by Hartmann *et al.*[11] are typically 0.6 MeV larger than those obtained in this work. For the only common target, namely carbon, this discrepancy is largely removed if we use the spectrum of Hartmann *et al.* reanalyzed to use the efficiencies calculated with the improved code of Cecil *et al.* If we extract the nuclear temperature from the adjusted spectrum of Hartmann *et al.*, we obtain a nuclear temperature of 2.3 MeV in agreement with our result of $(2.1 \pm 0.2)$ MeV for carbon. Hartmann *et al.* extracted a nuclear temperature of 2.71 MeV from their data. The difference between their original result and the value we obtain from the adjusted spectrum occurs because of differences in the assumed neutron detector efficiencies at low neutron energies between about 2 and 10 MeV. The good agreement of the nuclear temperature deduced from the adjusted spectrum with our result is another indication that the carbon measurements of Hartmann *et al.* generally agree with the carbon measurements presented here when a common efficiency calculation is used. We note also that Eisenegger *et al.*[28] reported nuclear temperatures for negative pions stopping in heavy nuclei which are consistent with the results presented here for Pb and Ta and somewhat smaller than the result reported for $^{197}$Au by Hartmann *et al.* The use of common efficiency calculations would tend to move the temperatures obtained for the data of Hartmann *et al.* for heavier targets into better agreement with the temperatures reported here. Presumably, common efficiency calculations applied to the recent results of Eisenegger *et al.* would also change the extracted nuclear temperatures. Since their results were reported only in an abstract, we cannot compare efficiency calculations.

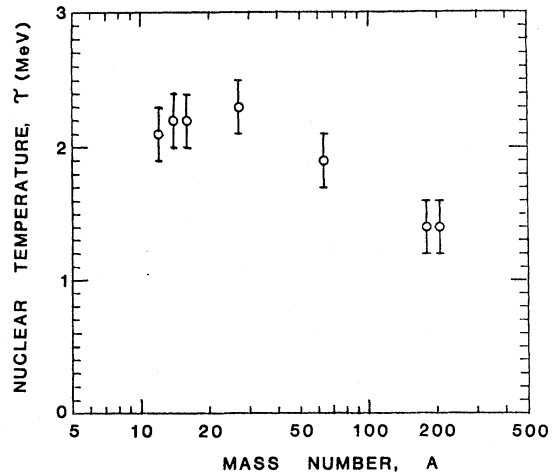


FIG. 9. Nuclear temperature versus the mass number of the target nucleus.

## VII. NEUTRON YIELDS AND KINETIC ENERGY OF NEUTRONS

In Table V, we present the yield of neutrons per pion stopped in targets of C, N, O, Al, Cu, Ta, and Pb. The yield above 1.2 MeV was obtained by integrating the measured spectrum in the region above 1.2 MeV. The number of neutrons emitted below 1.2 MeV was determined by extrapolating a least-squares fit to the measured evaporation spectrum and numerically integrating the Le Couteur expression from 0 to 1.2 MeV. Column 3 lists values of the total yield $N_T$ ($>0$ MeV). Columns 4 and 5 represent the decomposition of the total yield into an evaporation portion $N_e$ and a direct portion $N_d$. The evaporation yield is the integral of the fitted expression of Le Couteur; the yield of direct neutrons was obtained by subtracting the evaporation yield from the total yield. The uncertainties include an estimated uncertainty for the extrapolation

TABLE V. Yields of neutrons resulting from negative pion capture in various targets.

| Target | Threshold (MeV) | Yield above threshold | Total yield $N_T$ (>0 MeV) | Yield of evaporation neutrons $N_e$ | Yield of direct neutrons $N_d$ | Reference |
|---|---|---|---|---|---|---|
| $^{12}$C | 1.0 | 2.02 | 2.12±0.16 | 0.63 | 1.45±0.10 | Hartmann *et al.* (Ref. 11) |
| | 2.0 | | 2.5 ±0.3 | 0.83±0.08 | 1.6 ±0.3 | Klein *et al.* (Ref. 12) |
| | 1.2 | 2.26±0.17 | 2.44±0.18 | 0.67±0.13 | 1.77±0.15 | This work |
| | 1.0 | | 2.05 | 0.59 | 1.46 | Hartmann *et al.* (adjusted)[a] |
| | 2.0 | | 2.00 | 0.77 | 1.31 | Klein *et al.* (adjusted)[a] |
| $^{14}$N | 1.2 | 2.39±0.19 | 2.62±0.20 | 0.86±0.16 | 1.76±0.17 | This work |
| | | | 2.6 ±0.3 | 0.9 ±0.09 | 1.7 ±0.3 | Klein *et al.* |
| $^{16}$O | 1.2 | 2.41±0.19 | 2.63±0.20 | 0.85±0.15 | 1.78±0.16 | This work |
| | | | 2.7 ±0.3 | 0.99±0.10 | 1.7 ±0.3 | Klein *et al.* |
| $^{27}$Al | 1.2 | 2.83±0.26 | 3.21±0.29 | 1.55±0.26 | 1.67±0.23 | This work |
| $^{59}$Co | 1.0 | 3.58 | 4.04 ±0.24 | | 1.38±0.11 | Hartmann *et al.* |
| | 0.0 | 4.5 ±0.2 | 4.5 ±0.2 | | | Pruys *et al.* (Ref. 29) |
| $^{63.5}$Cu | 1.2 | 4.02±0.55 | 5.04±0.61 | 3.32±0.61 | 1.72±0.51 | This work |
| $^{181}$Ta | 1.2 | 5.47±1.19 | 7.95±1.39 | 6.15±1.14 | 1.80±1.14 | This work |
| $^{197}$Au | 1.0 | 4.95 | 6.31±0.36 | | 1.32±0.10 | Hartmann *et al.* |
| | 0.0 | 6.6 ±0.4 | 6.6 ±0.4 | | | Pruys *et al.* |
| $^{208}$Pb | 1.2 | 5.87±1.41 | 8.86±1.66 | 7.19±1.69 | 1.67±1.37 | This work |
| $^{209}$Bi | 0.0 | 6.8 ±0.4 | 6.8 ±0.4 | | | Pruys *et al.* |

[a]Neutron spectrum adjusted to incorporate neutron detector efficiencies calculated using the computer code of Cecil *et al.* (see text).

to zero energy with the fitted Le Couteur expression, which includes the ±0.2 MeV uncertainty in the extracted temperatures. For the direct portion of the spectrum, the number of neutrons per stopped pion is substantially constant for all the targets with a mean value of 1.74±0.13.

In Table V, we present also the neutron yields determined in some other recent measurements for comparison on common or similar targets. Included are the results for the readjusted data of Hartmann *et al.*[11] and Klein *et al.*[12] on carbon based on the efficiency calculations with the code of Cecil *et al.*, as discussed in Sec. V. The total yield ($N_T$=2.44±0.18) determined in this work for carbon presented in Table V agrees with the value reported by Klein *et al.*[12] ($N_T$=2.5±0.3) and overlaps with the value ($N_T$=2.12±0.16) reported by Hartmann *et al.*[11] The lower neutron yields of the adjusted spectra of Hartmann *et al.* and Klein *et al.* result primarily from the lower yield in the intermediate-energy region (10 to 40 MeV) of Hartmann *et al.* and in the higher-energy region of Klein *et al.*, respectively. (These differences are most strongly reflected in the "direct" yields.) Using an activation $\gamma$-ray technique, Pruys *et al.*[29] reported measurements of the total number of neutrons and protons emitted following negative-pion capture in targets of $^{59}$Co, $^{75}$As, $^{197}$Au, and $^{209}$Bi. Their result for $^{59}$Co of 4.5±0.2 neutrons per stopped pion is slightly larger than the 4.0±0.2 reported by Hartmann *et al.* for the same target. We can compare the activation result with our result for Cu if we adjust their result to reflect the general trend that the observed yields increase approximately as $A^{1/2}$. Using this dependence to provide a first-order correction, we see that the result of Pruys *et al.* for $^{59}$Co implies a value of 4.7±0.2 for $^{63.5}$Cu which agrees (within uncertainties) with our result of 5.0±0.6.

The results reported here for the total integrated neutron yields (per stopped pion) for Ta and Pb are about 25% larger than the results reported by Hartmann *et al.*[11] for $^{197}$Au and by Pruys *et al.*[29] for $^{197}$Au and $^{209}$Bi. It is important to note that for these heavy nuclei a large fraction of the total neutron yield comes from the low-energy neutrons; for example, more than one third of our total yield for lead comes from the extrapolated region below the detection threshold. Note that 80% of the total yield from lead comes from the evaporation region.

Most of the observed difference with the result of Hartmann *et al.* is in the low-energy region; the total yields above about 5 MeV agree to better than 10%. The low-energy region of the neutron spectrum is most sensitive to residual background problems and relative errors in the efficiency calculations. The former occurs because high-energy neutrons scattered from floors, walls, and shielding will contaminate the low-energy portion of the spectrum. Hartmann *et al.* reported large room-scattered backgrounds which they subtracted with shadow-bar measurements. The present measurements, as noted in Sec. V, could suffer from some residual room-scattered background at neutron energies below 8 MeV; in addition, neutron detector efficiency calculations are known to be less reliable at neutron energies close to the detection threshold, where the efficiency changes rapidly as a function of energy. Because of the relatively large neutron yields at low energies for the heavy nuclei, such results are more sensitive to these problems than are results for lighter nuclei.

Clearly, the number of direct neutrons emitted per stopping pion is consistent with absorption on a quasideuteron plus some interactions of the two resulting neutrons with the final nucleus. We note also that this number can be understood in terms of the isobar doorway model[30] which gives a good account of the inverse (pion production) process in nucleon-nucleon reactions.[31] Although the isobar model is most relevant near the (3,3) resonance, the prediction of the isobar model still gives a good account of the direct neutron production from stopped pions. According to the isobar doorway model, pion absorption may be visualized as a two-step process: The pion combines with a nucleon to form an intermediate state $\Delta(3,3)$ isobar and then the $\Delta$ interacts with another nearby nucleon to yield two scattered nucleons in the final state. Since the $\Delta$ has a propagation distance of about 0.7 fm, the $\Delta$ isobar formed by the interaction of the captured pion with the first nucleon will interact only with a nearest-neighbor nucleon of the first nucleon; accordingly, negative pion capture by a finite nucleus should, in first approximation, be similar to pion capture by an alpha particle. We use the isobar doorway model to estimate the number of direct neutrons emitted per pion capture by an alpha particle.

The pion capture process in this model can be written as

$$\pi^- + N_1 + N_2 \xrightarrow{(\sigma)} \Delta + N_2 \xrightarrow{(\sigma')} 2N \ . \tag{4}$$

The negative pion can combine either with a proton or a neutron to produce a $\Delta^0$ or a $\Delta^-$:

$$\pi^- + p \rightarrow \Delta^0 (T=\tfrac{3}{2}, T_z=-\tfrac{1}{2}) \ , \tag{5}$$

$$\pi^- + n \rightarrow \Delta^- (T=\tfrac{3}{2}, T_z=-\tfrac{3}{2}) \ . \tag{6}$$

The number of neutrons per negative pion capture by an alpha particle can then be found from the relative neutron yields for the different possible isobar interactions as indicated in Table VI. The relative number of processes which will yield two neutrons per pion capture is seen to be $4+36=40$ and the number of processes which will yield one neutron is 4. Thus, from this model, we expect the average number of direct neutrons emitted per pion capture to be

$$N = \frac{(2)(40)+(1)(4)}{40+4} = 1.91 \ . \tag{7}$$

This prediction compares with our measured average number of emitted direct neutrons of $1.74 \pm 0.28$. We expect the predicted number to be too high because it ignores loss of neutrons from the direct portion of the spectrum to the evaporation portion. The large multiplicity of evaporation neutrons for a heavy target like lead requires that some of the direct neutrons be absorbed by the nucleus.

In Table VII, we list our results for the total kinetic energy carried away by the neutrons as well as for the distribution of kinetic energy between the direct and the evaporation portions of the spectrum. The relative contributions of direct and evaporation processes are determined similar to the yield contributions. We note that it is important to consider the kinematic maximum neutron energy in determining the proper centroid energy to associate with the highest energy bin in a neutron spectrum. This consideration can affect the total integrated neutron energy by $\lesssim 2$ MeV. The kinetic energy carried away by the evaporation neutrons increases monotonically with the mass number $A$ from 1.9 MeV for carbon up to 13.3 MeV for lead. Results in Table VII indicate that direct neutrons from light targets carry away more energy than neutrons from medium or heavy targets. Typical values are 76 MeV for carbon, 67 MeV for copper, and 65 MeV for lead. The decrease with mass number in the observed values of the energy carried away by direct neutrons results from an increased collision probability of the outgoing neutrons with other nucleons inside the nucleus. The energy lost by the collision of a direct neutron is shared by the remaining nucleons and

TABLE VI. Relative neutron yields for the different available Δ-isobar reactions in negative pion capture by an alpha particle.

$$\pi + N_1 + N_2 \overset{(\sigma)}{\rightleftarrows} \Delta + N_2 \overset{(\sigma')}{\rightleftarrows} 2N$$

| $\Delta+N_2$ | No. $N_1$ | Relative cross section[a] $\sigma$ | No. $N_2$ | Relative cross section[a] $\sigma'$ | Net number of possibilities | Number of direct neutrons | Relative yield |
|---|---|---|---|---|---|---|---|
| $\Delta^0+n$ | 2 | 1 | 2 | 1 | 4 | 2 | 8 |
| $\Delta^0+p$ | 2 | 1 | 1 | 2 | 4 | 1 | 4 |
| $\Delta^-+p$ | 2 | 3 | 2 | 3 | 36 | 2 | 72 |

[a]From isospin Clebsch-Gordan coefficients.

contributes to the excitation of the residual nucleus. The observed constancy in the *number* of direct neutrons indicates that the effect of the energy loss by collision of the outgoing neutron with other nucleons does not reduce the population of the neutrons in the direct portion of the spectrum.

The kinetic energies carried away by neutrons are compared in Table VIII for C, N, O, Al, Cu, Ta, and Pb with values reported by others. Our measurements reveal that the emitted neutrons per pion captured in carbon carry away 77.5±4.9 of kinetic energy which is significantly higher than the 68 MeV reported by Anderson *et al.*, but lower than the 110 MeV value reported by Hattersley *et al.* Our value agrees with the value of Hartmann *et al.* for carbon as originally reported. If we adjust the value of Hartmann *et al.* for a common efficiency calculation with this work, their value falls to about 73.5±5.5 MeV, still in agreement (within uncertainties) of the value reported here. Note that the values reported here for C, N, O, Al, Cu, and Pb are consistently (and significantly) lower than the values reported by Hattersley *et al.*

TABLE VII. Kinetic energy carried away by neutrons emitted as a result of negative pion capture in various targets.

| Target | Neutron kinetic energy (in MeV) Evaporation | Direct | Total |
|---|---|---|---|
| C | 1.9±0.6 | 75.6±4.8 | 77.5±4.9 |
| N | 2.5±0.7 | 73.7±4.7 | 76.2±4.9 |
| O | 2.5±0.7 | 75.6±4.8 | 78.1±5.0 |
| Al | 4.7±1.2 | 68.3±4.5 | 73.0±4.8 |
| Cu | 8.4±2.5 | 67.3±4.9 | 75.6±5.4 |
| Ta | 11.7±4.6 | 66.7±6.1 | 78.4±6.7 |
| Pb | 13.3±5.4 | 65.1±6.5 | 78.4±7.2 |
| | | Average | 76.7±2.0 |

## VIII. COMPARISON WITH THEORETICAL CALCULATIONS

The detailed mechanism responsible for the emission of neutrons by stopping pions is still not well understood.[32] Various models have been proposed to account for the neutron production. Guthrie *et al.*[1] studied the reactions resulting from negative pion capture in light elements using a Monte Carlo intranuclear cascade model[33] and compared their calculations to the measurements of Anderson *et al.*[5] for carbon and aluminum. Bertini[2] published a more detailed evaluation of the intranuclear cascade model,[33,34] and he noted that the model predicted too soft a neutron spectrum for a heavy target such as lead. Bertini made several spectral comparisons with previous measurements[5–7] for various targets. The neutron energy spectra calculated by Bertini disagree with the data of Hattersley *et al.* in the region above about 10 MeV, and they disagree also with our data. The disagreement worsens for heavy elements where the model predicts too soft a neutron spectrum. Iljinov *et al.*[3] introduced refinements to the intranuclear cascade calculation, utilized the exciton model[35,36] to describe the preequilibrium decay, and compared their calculation to the measurements of Anderson *et al.* and Venuti *et al.* for lead. Iljinov *et al.* noted that the inclusion of preequilibrium decay improves the agreement between the calculation and the experimental measurements of Anderson *et al.* in the region where the evaporation and direct spectra overlap. Gadioli *et al.*[4] used the preequilibrium model to predict yields of neutrons and charged particles produced by stopping pions. Gadioli *et al.* did not

TABLE VIII. Comparison with values reported by other authors of the kinetic energy carried away by neutrons emitted as a result of negative-pion capture in various targets.

| Target | Total neutron kinetic energy[a] (MeV) | Authors |
|---|---|---|
| C | 77.5 ± 4.9 | This work |
| | 68 | Anderson *et al.* |
| | 110 ± 11 | Hattersley *et al.* |
| | 56.2 | Dey *et al.* |
| | 76.0 ± 5.7 | Hartmann *et al.* |
| | 73.5 ± 5.5 | Hartmann *et al.*[b] |
| | 76 ± 9 | Klein *et al.* |
| | 72 ± 8 | Klein *et al.*[b] |
| N | 76.2 ± 4.9 | This work |
| | 100 ± 10 | Hattersley *et al.* |
| | 78 ± 10 | Klein *et al.* |
| O | 78.1 ± 5.0 | This work |
| | 105 ± 12 | Hattersley *et al.* |
| | 79 ± 10 | Klein *et al.* |
| Al | 73.0 ± 4.8 | This work |
| | 74 | Anderson *et al.* |
| | 100 ± 12 | Hattersley *et al.* |
| Cu | 75.6 ± 5.4 | This work |
| | 123 ± 12 | Hattersley *et al.* |
| Ta | 78.4 ± 6.7 | This work |
| Pb | 78.4 ± 7.2 | This work |
| | 100 ± 12 | Hattersley *et al.* |

[a]Uncertainties shown for our data are experimental uncertainties which were obtained from the statistical uncertainties and systematic uncertainties summed quadratically.
[b]For adjustment of data of Hartmann *et al.* and Klein *et al.*, see discussion in text.

make comparisons with experimental measurements but reported that the calculated neutron yield from a copper target agreed well with the measurements of Hattersley *et al.*

In Fig. 10, we compare our neutron spectrum from oxygen with the Monte Carlo intranuclear cascade model calculation of Guthrie *et al.*[1] The calculation predicts a deficiency of neutrons above 30 MeV and below about 2 MeV, and an excess of neutrons in the region from about 2 to 20 MeV. It should be noted that in the Monte Carlo calculation the incident pions are assumed to travel along parallel paths uniformly distributed over the cross-sectional area of the nucleus. It was assumed also that pions orbiting the nucleus will be absorbed by the nucleus in the same manner as a parallel beam of pions. In Fig. 11, we compare our neutron spectra from lead with two Monte Carlo calculations. The dashed-line histogram is the calculation of Gadioli *et al.*[4,37] There is good agreement in the region below 10 MeV. There is a large discrepancy

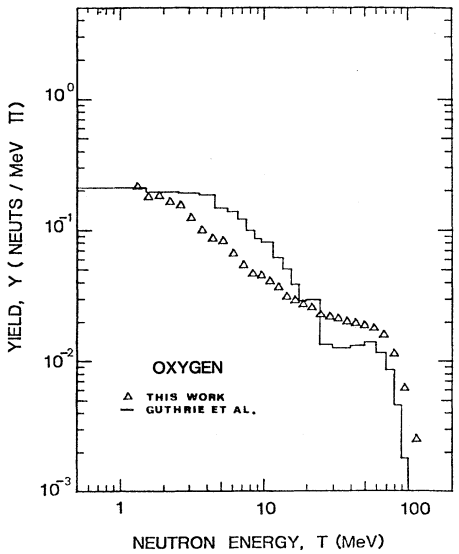


FIG. 10. Comparison of the measured spectrum of neutrons from negative pions stopping in oxygen with the calculated spectrum of Guthrie *et al.* (Ref. 1).

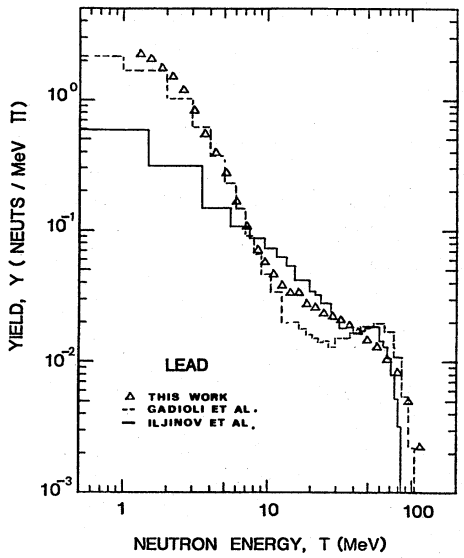


FIG. 11. Comparison of the measured spectrum of neutrons from negative pions stopping in lead with the calculated spectra of Gadioli *et al.* (Ref. 4) and Iljinov *et al.* (Ref. 3).

between our measured spectrum and the calculation of Gadioli *et al.* in the region between 10 and about 40 MeV; moreover, the calculation predicts a small bump in the region around 60 MeV which we do not observe in our measured spectrum. The solid line histogram is the calculation of Iljinov *et al.*[3,38] In the region between about 30 and 80 MeV, the calculations of Iljinov *et al.*[3,38] correlate with our data better than other published calculations.

Each of the three calculations mentioned includes the two-nucleon absorption mechanism; in addition, Iljinov *et al.* include absorption by quasialpha clusters about 25 percent of the time. Also Iljinov *et al.* consider that pion absorption occurs predominantly at the nuclear surface rather than throughout the nuclear volume. Bertsch and Riska[39] lend support to the assumption made by Iljinov *et al.* of pion absorption by alpha clusters. Bertsch and Riska attempt to explain pion absorption at threshold with the assumption that the dominant mechanism is the absorption of a virtual pion, which is created in a scattering of the initial physical pion. They conclude that, while the model is successful in the case of the deuteron, only 70 to 90 percent of the pion absorption rates in other nuclei as deduced from pionic atom level widths may be explained by the two-nucleon absorption mechanism involving pion rescattering. They attribute the 10 to 30 percent discrepancy to a many-body absorption process.

Jackson *et al.*[40] reported possible evidence for multinucleon-absorption modes from their study of the pion-absorption mechanism in $^4$He. For 220 MeV pions on $^4$He, Jackson *et al.* observed a rising yield of lower-energy protons in the spectrum at 45°, and they observed that the yield of these lower-energy protons was 3.6 times higher with incident positive pions than with incident negative pions. Based on the fact that the calculated ratio is 3 for four-body absorption and 7.6 for quasifree pion-nucleon scattering, they attributed these lower-energy protons to the four-nucleon absorption process.

We note that the yield of direct neutrons from all targets increases as the neutron energy decreases down to about 10 MeV. Dey *et al.* observed similar behavior in their direct neutron spectra from carbon and holmium. Also they indicated that the presence of low-energy neutrons in their direct neutron spectra could indicate absorption by heavier clusters. From our analysis of our carbon spectrum, we observe that the neutron yield from the direct portion of the carbon spectrum starts to increase at a neutron kinetic energy of about 30 MeV as the neutron kinetic energy decreases. Assuming only absorption on alpha clusters, Kolybasov[41] calculated the neutron spectrum from negative pion absorption in carbon and found that the spectrum peaked in the region around 20 MeV. This peaking is in contrast to an expected deficiency of neutrons in this energy region on the basis of the two-nucleon absorption mechanism. An enhancement of the yield in the region below 30 MeV in the direct portion of the spectrum seems to support the view that absorption by clusters larger than two nucleons is not negligible. Lee *et al.*[42] reported evidence for absorption by alpha clusters as a result of their measurements of correlated neutron-deuteron and neutron-triton emission after pion capture on $^{12}$C. Lee *et al.* measured the energy of each member of a neutron-deuteron and a neutron-triton pair and the opening angle between the neutron and the charged particle. They observed a strong peaking at an opening angle of 180°. Also the measured energy spectra of deuterons and tritons in coincidence with neutrons agreed with calculations of Kolybasov.

## IX. CONCLUSIONS

We measured the energy spectra and yields of neutrons emitted following the nuclear capture of negative pions in C, N, O, Al, Cu, Ta, and Pb,

decomposed each spectrum into an evaporation portion and a direct portion. The measurements reported here have large discrepancies with measurements performed before the meson factories became operational, but are in better agreement with the more recent measurements of Hartmann *et al.*[11] and Klein *et al.*[12] The remaining discrepancies are attributed to the energy resolutions, efficiency calculations, the ability to reject $\gamma$ rays, and the presence of target-correlated backgrounds. The agreement at neutron energies above about 30 MeV is improved through the use of common efficiency calculations to reanalyze the results of Hartmann *et al.* and Klein *et al.*

More specifically, the following conclusions can be made regarding the spectra and yields of neutrons:

(1) The neutron spectrum from a light target displays a shoulder in the region around 60 MeV which is consistent with a two-nucleon absorption mechanism.

(2) The direct neutron spectra are characterized by a rising yield as the neutron energy decreases in the region from about 30 MeV down to about 10 MeV.

(3) The number of direct neutrons per pion capture is the same for all the targets studied. The mean vlaue is $1.74 \pm 0.28$.

(4) The number of evaporation neutrons per pion capture increases by an order of magnitude from about 0.7 for carbon to about 7 for lead.

(5) The total kinetic energy carried away by the neutrons is the same for all the targets studied; the mean value is $76.7 \pm 2.5$ MeV. The kinetic energy carried away by evaporation neutrons increases with the mass number of the target with an associated decrease in the kinetic energy carried away by direct neutrons.

We compared our measurements with three calculations and found agreement over limited spectral regions in two cases and no agreement in a third case. The preequilibrium calculation of Iljinov *et al.*[3] for a lead target predicts a neutron spectrum in agreement with our measured spectra in the region between about 30 and 80 MeV. This calculation assumes that 75 percent of the pion absorption is on two nucleons and that 25 percent is on alpha clusters. The calculations of Gadioli *et al.*[4] give a good representation of the evaporation spectrum below 10 MeV. The intranuclear cascade calculations of Guthrie *et al.*[1] for pion absorption on light nuclei do not agree with our experimental data.

## ACKNOWLEDGMENTS

We are grateful to Professor E. Gadioli and Dr. P. M. Hattersley for sending us their unpublished spectra. We are indebted also to the Nevis Laboratories of Columbia University for use of the synchocyclotron, and the cyclotron staff for their cooperation. We thank Dr. Peter Tandy for useful discussions, and Dr. H. E. Jackson and Dr. J. P. Schiffer for information relating to the isobar doorway model. This work was supported in part by the National Institutes of Health under Grant CA-14375 and the Energy Research and Development Administration under Contract EY-76-S-02-2231.

*Present address: Department of Physics, ChiangMai University, Chiangmai, Thailand.

†Present address: Cyclotron Laboratory, University of Manitoba, Winnipeg, Manitoba, Canada.

‡Present address: Sperry Univac, Dahlgren, Virginia 22448.

§Present address: Department of Radiation Therapy and Nuclear Medicine, Thomas Jefferson University, Philadelphia, Pennsylvania 19107.

[1]M. P. Guthrie, R. G. Alsmiller, Jr., and H. W. Bertini, Nucl. Instrum. Methods 66, 29 (1968); Errata, Nucl. Instrum. Methods 91, 669 (1971).

[2]H. W. Bertini, Phys. Rev. C 1, 423 (1970).

[3]A. S. Iljinov, V. I. Nazaruk, and S. E. Chigrirov, Nucl. Phys. A 268, 513 (1978).

[4]E. Gadioli and E. Gadioli Erba, Nucl. Phys. A 256, 414 (1976).

[5]H. L. Anderson, E. P. Hincks, C. S. Johnson, C. Rey, and A. M. Segar, Phys. Rev. 133, B392 (1964).

[6]G. Campos Venuti, G. Fronterotta, and G. Matthial, Nuovo Cimento 34, 1446 (1964).

[7]P. M. Hattersley, M. Muirhead, and J. N. Woulds, Nucl. Phys. 67, 309 (1965); private communication.

[8]W. Dey, R. Engfer, H. Guyer, R. Hartmann, E. A. Hermes, H. P. Isaak, J. Morgenstern, H. Muller, H. S. Pruys, W. Reichart, and H. K. Walter, Helv. Phys. Acta 49, 778 (1976); H. P. Isaak, thesis, Eidgenossische Technische Hochschule, Zurich, 1976.

[9]K. A. Brueckner, R. Serber, and K. M. Watson, Phys. Rev. 84, 258 (1951).

[10]A. G. Barkow, O. E. Edmund, R. E. Penarande, G. Kane, and Z. O'Frich, Nuovo Cimento 28, 673 (1963).

[11]R. Hartmann, H. P. Isaak, R. Engfer, E. A. Hermes, H. S. Pruys, W. Dey, H. J. Pfeiffer, U. Sennhauser, H. K. Walter, and J. Morgenstern, Nucl. Phys. A 300, 345 (1978).

[12]U. Klein, G. Buche, W. Kluge, H. Matthay, and G. Mechtersheimer, Nucl. Phys. A 329, 339 (1979).
[13]R. Madey and F. M. Waterman, Nucl. Instrum. Methods 106, 89 (1973).
[14]R. Madey, F. M. Waterman, and A. R. Baldwin, Nucl. Instrum. Methods 133, 61 (1976).
[15]T. K. Alexander and F. S. Goulding, Nucl. Instrum. Methods 13, 244 (1961).
[16]D. A. Gedeke and C. W. Williams, Ortec report, 1968.
[17]H. H. Knox and T. G. Miller, Nucl. Instrum. Methods 101, 519 (1972).
[18]B. D. Anderson, A. R. Baldwin, A. M. Kalenda, R. Madey, J. W. Watson, C. C. Chang, H. D. Holmgren, R. W. Koontz, and J. R. Wu, Phys. Rev. Lett. 46, 226 (1981).
[19]R. A. Cecil, B. D. Anderson, A. R. Baldwin, R. Madey, W. Schimmerling, J. W. Kast, and D. Ortendahl, Phys. Rev. C. 24, 2013 (1981).
[20]R. Cecil, B. D. Anderson, and R. Madey, Nucl. Instrum. Methods 161, 439 (1979).
[21]N. Stanton, Chicago Operations Office Report COO-1545-92, 1971.
[22]F. P. Brady and J. L. Romero, University of California at Davis-Crocker Nuclear Laboratory Report UCD—CNL 192, 1979, p. 171; private communication.
[23]D. A. Kellogg, Phys. Rev. 90, 224 (1953).
[24]V. V. Verbinski, W. R. Burrus, T. A. Love, W. Zobel, and N. W. Hill, Nucl. Instrum. Methods 65, 8 (1968).
[25]J. B. Czirr, D. R. Nygren, and C. D. Zafiratos, Nucl. Instrum. Methods 31, 226 (1964).
[26]R. Madey, F. M. Waterman, A. R. Baldwin, J. N. Knudson, J. D. Carlson, and J. Rapaport, Nucl. Instrum. Methods 151, 445 (1978).
[27]K. J. Le Couteur, Proc. Phys. Soc. London 65, 718 (1952).
[28]C. Eisenegger, R. Engfer, R. Hartmann, E. Hermes, H. Isaak, T. Koslowski, H. Pfeiffer, H. Pruys, F. Schleputz, V. Sennhauser, H. Walter, and A. Zylinski, Proceedings of the International Conference on Nuclear Physics, Berkeley, California, 1980, p. 718.
[29]H. S. Pruys, R. Engfer, R. Hartmann, V. Sennhauser, H. J. Pfeiffer, H. K. Walter, J. Morgenstern, A. Wyttenbach, E. Gadioli, and E. Gadioli-Erba, Nucl. Phys. A 316, 365 (1979).
[30]E. J. Moniz, *Proceedings of Theoretical Methods in Medium-Energy and Heavy-Ion Physics,* edited by K. W. McVoy and W. A. Friedman (Plenum, New York, 1978), p. 603.
[31]L. Kisslinger and W. Wang, Ann. Phys. (N.Y.) 99, 374 (1976).
[32]F. Scheck, in *Nuclear and Particle Physics at Intermediate Energies,* edited by J. B. Warren (Plenum, New York, 1976), p. 305.
[33]H. W. Bertini, Phys. Rev. 131, 1801 (1963).
[34]H. W. Bertini, Phys. Rev. 138, AB2 (1965).
[35]J. J. Griffin, Phys. Rev. Lett. 17, 478 (1966).
[36]M. Blann, Phys. Rev. Lett. 21, 357 (1968).
[37]E. Gadioli, private communication.
[38]Iljinov *et al.* did not report a normalization factor for their theoretical calculations. We took the normalizatioin factor from their reported comparison with the measurement of Anderson *et al.* to be 2.1 which was the ratio of the spectrum reported by Anderson *et al.* as presented by Iljinov *et al.*
[39]G. F. Bertsch and D. O. Riska, Phys. Rev. C 18, 317 (1978).
[40]H. E. Jackson, S. L. Tabor, K. E. Rehm, J. P. Schiffer, R. E. Segal, L. L. Rutledge, Jr., and M. A. Yates, Phys. Rev. Lett. 39, 1601 (1977).
[41]V. M. Kolybasov, Yad. Fiz. 3, 729 (1966) [Sov. J. Nucl. Phys. 3, 704 (1966)].
[42]D. M. Lee, R. C. Minehart, S. E. Sobottka, and K. O. H. Ziock, Nucl. Phys. A 197, 106 (1972).